

The X-ray jet and central structure of the active galaxy NGC 315

D.M. Worrall, M. Birkinshaw & M.J. Hardcastle

Department of Physics, University of Bristol, Tyndall Avenue, Bristol BS8 1TL

13 November 2018

ABSTRACT

We report the *Chandra* detection of resolved X-ray emission of luminosity 3.5×10^{40} ergs s^{-1} (0.4–4.5 keV) and power-law energy spectral index $\alpha = 1.5 \pm 0.7$ from a roughly 10 arcsec length of the north-west radio jet in NGC 315. The X-ray emission is brightest at the base of the radio-bright region about 3 arcsec from the nucleus, and is consistent with a synchrotron origin. At a projected distance of 10 arcsec from the core, the jet is in approximate pressure balance with an external medium which is also detected through its X-ray emission and which has $kT \approx 0.6 \pm 0.1$ keV, consistent with earlier *ROSAT* results. The high spatial resolution and sensitivity of *Chandra* separates nuclear unresolved emission from the extended thermal emission of the galaxy atmosphere with higher precision than possible with previous telescopes. We measure an X-ray luminosity of 5.3×10^{41} ergs s^{-1} (0.4–4.5 keV) and a power-law energy index of $\alpha = 0.4 \pm 0.4$ for the nuclear component.

Key words: galaxies:active – galaxies:individual: NGC 315– galaxies: jets – radiation mechanisms: non-thermal – X-rays:galaxies

1 INTRODUCTION

X-ray studies of the kpc-scale radio jets of active galaxies can test whether their electrons are accelerated to high energies. Fast synchrotron energy losses of high-energy electrons allow X-ray maps to pinpoint the acceleration sites. Nearby, low-power jets of the Fanaroff & Riley (1974) class I (FRI) have large projected angular sizes, and provide the best opportunity for measuring X-ray substructure.

The high spatial resolution and sensitivity of *Chandra* have been crucial to extending X-ray jet studies beyond Cen A and M 87, the only FRI radio galaxies for which resolved X-ray jets had been detected prior to its launch (Schreier et al. 1979; Schreier, Gorenstein & Feigelson 1982). In this paper we report the detection of an X-ray jet in the inner parts of the giant FRI radio galaxy NGC 315, at $z = 0.0165$.

The observation was made as part of our *Chandra* programme of imaging and spectroscopy of FRI radio galaxies from the B2 bright sample (Colla et al. 1975; Ulrich 1989), aimed at studying the validity of the unification of B2 radio galaxies and BL Lac objects and at testing physical and dynamical models for the X-ray and radio-emitting structures. NGC 315 is one of the X-ray brightest B2 sources studied with *ROSAT* (Canosa et al. 1999), and consequently only a short *Chandra* exposure time was needed to meet our criterion of uniform data quality for the sample.

NGC 315 has a two-sided radio structure extending roughly one degree on the sky (Bridle et al. 1979). On milliarcsec scales, the sidedness asymmetry and proper motions suggest the jet bulk motion is relativistic ($v > 0.75c$), possibly accelerating between 3 and 10 pc from the nucleus, with an angle to the line of sight between 30 and 40 degrees (Cotton et al. 1999; Giovannini et al.

1994, 2001). The north-west radio jet remains dominant on a scale of a few tens of arcsec. A transition from supersonic to turbulent transonic flow, with deceleration by entrainment, is likely to occur at about 17 arcsec from the core, where there is a sudden change in jet opening angle (Bicknell 1986). Bicknell (1994) shows from the application of conservation laws that an entraining jet which is initially relativistic will have a speed between 0.3 and 0.7 c at the flare point, and he demonstrates how such a model is consistent with the radio data from NGC 315.

Resolved jet emission from NGC 315 remains unseen in the optical from ground-based (Butcher et al. 1980) and *HST* (Verdoes Kleijn et al. 1999) measurements. The *HST* observations detect an unresolved nuclear source surrounded by an inclined, regular, circum-nuclear disk of radius about 1 arcsec and extinction about 0.25 magnitudes, whose axis is aligned to within a few degrees of the north-west radio jet (Verdoes Kleijn et al. 1999; de Ruiter et al. 2002).

In this paper we adopt a value for the Hubble constant of $H_o = 70$ km s^{-1} Mpc $^{-1}$. 1 arcsec corresponds to 335 pc at NGC 315. The J2000 position of the radio nucleus is $\alpha = 00^{\circ}57'48''.8834$. $\delta = +30^{\text{h}}21^{\text{m}}08^{\text{s}}.812$ (Xu et al. 2000). The Galactic column density to the source obtained from 21 cm measurements is 5.92×10^{20} cm $^{-2}$ (Dickey & Lockman 1990), and local absorption through this gas is included in all our spectral models.

2 *Chandra* OBSERVATIONS AND RESULTS

We observed NGC 315 with the back-illuminated CCD chip, S3, of the Advanced CCD Imaging Spectrometer (ACIS) on board *Chandra* on 2000 October 8. Details of the instrument and its modes

arXiv:astro-ph/0307031v1 1 Jul 2003

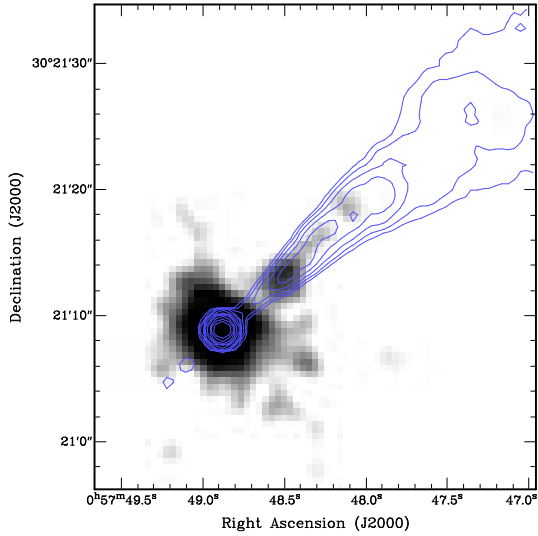


Figure 1. The grey-scale image shows the 0.5–5 keV *Chandra* data for NGC 315, in $0.492''$ bins and smoothed with a Gaussian of $\sigma = 0.74''$. The contours (in factors of two increment) outline the radio jet from a high-resolution 5 GHz VLA image (Cotton, 2002, private communication) which has been convolved with a Gaussian of $\sigma = 1''$ in order to match the resolution of the X-ray image. Jet X-ray emission is seen, particularly at the base of the first radio enhancement. Low surface-brightness X-ray emission is suppressed in this image.

of operation can be found in the *Chandra* Proposers’ Observatory Guide, available from <http://cxc.harvard.edu/proposer>. The observation was made in the VFaint data mode, with a 128-row subarray (giving a 1 by 8 arcmin field of view, with the source roughly centred in the 1 arcmin direction and at a 3:1 offset position in the 8 arcmin direction). The use of the subarray was to reduce the read-out time to 0.44 s in order to guard against the effects of pile-up should much of the flux detected with *ROSAT* (Worrall & Birkinshaw 1994) be unresolved to *Chandra*. Results presented here all use CIAO v2.3 and the CALDB v2.20 calibration database. The data have been re-calibrated and analysed, with random pixelization removed and taking advantage of VFaint background cleaning, following the software ‘threads’ from the *Chandra* X-ray Center (<http://cxc.harvard.edu/ciao>). Events with grades 0,2,3,4,6 are used. All X-ray spectra are binned to a minimum of 20 counts per bin, and the time-dependent decline in quantum efficiency is taken into account using the recommended methods. After the VFaint background cleaning, there were no time intervals which needed to be excluded because of anomalously high background, and the calibrated data have an observation duration of 4.67 ks.

2.1 The X-ray image and resolved jet

Fig. 1 shows the 0.5–5 keV *Chandra* X-ray data together with contours outlining the inner radio emission. In the figure, the X-ray core is burned out and the low-surface-brightness emission is suppressed in order to emphasize small-scale extended emission.

X-ray emission from the core is extended with a similar ellipticity and position angle to the optical emission from NGC 315. We have used the IRAF STSDAS task ELLIPSE to measure the ellipticity of a Kitt Peak 4 m R-band image (Birkinshaw and Davies, private communication), and find position angles between 40 and 46 degrees and ellipticities between 0.16 and 0.26 for most of the galaxy. For example, at a semi-major axis of 10 arcsec, the elliptic-

ity is 0.251 ± 0.002 and the position angle is 45.2 ± 0.2 degrees. We find an ellipticity of 0.29 ± 0.03 and a position angle of 49 ± 3 when similar procedures are applied to the 0.5–5 keV X-ray image smoothed with a Gaussian of $\sigma = 1.3$ arcsec, masking out the region of the resolved jet.

Resolved X-ray emission from the NW radio jet is clearly evident at a position angle roughly perpendicular to the semi-major axis of the galaxy. The X-ray emission is particularly strong at the base of the first radio enhancement. We find 55 ± 9 net counts in the energy range 0.5 – 5 keV from the jet as measured in a rectangular box of length 12 arcsec and width 6 arcsec, starting 3 arcsec from the nucleus, taking a corresponding box diametrically opposite the nucleus to measure the background.

2.2 Radial-Profile Analysis

In order to separate unresolved and galaxy emission, avoiding resolved jet emission, we extracted a source-centred 0.4–7 keV radial profile excluding a pie slice of position angle between 295° and 325° . We fitted the profile with models convolved with the Point Response Function (PRF), using home-grown software whose algorithms are described in Birkinshaw (1994). Our procedure for finding the appropriate energy-weighted PRF follows that described in Worrall et al. (2001), except that we used a revised functional form for the third additive component in order to give an improved description of bright point sources (see <http://cxc.harvard.edu/cal/Hrma/psf>): for the energy distribution of the counts in our NGC 315 observation we find this third component to be proportional to $(1 + \theta/0.021)^{-2.1}$, for $\theta \leq 5$ arcmin.

The *ROSAT* PSPC measured thermal X-ray emission associated with NGC 315’s atmosphere out to a radius of 2 arcmin, and we expect this emission to dominate over the background throughout part of the field of view of our *Chandra* observation. A rectangular box of size 1 arcmin by 2 arcmin as far from NGC 315 as possible but still in the field of view (i.e. all being 4 arcmin or more away from the nucleus of NGC 315) contains 0.007 ± 0.001 cts arcsec $^{-2}$, 0.4–7 keV, consistent with time-averaged results available from http://cxc.harvard.edu/cal/Acis/Cal_prods/bkgnd/current. We use this as a measure of the background in the observation for all the analyses presented here. As a check, we have also performed the radial analysis allowing our fitting to find the best-fitting source and background contributions to an annulus of radii 40 and 62 arcsec, and the results for the background and the model parameters agree with those using the rectangular-box background.

The radial profile gives unacceptable fits to single-component models of a point source or a β model (used to describe gas in hydrostatic equilibrium), but the fit to the combination of the two is good, as shown in Fig. 2. Parameter values and uncertainties are given in Table 1.

2.3 X-ray Spectrum

Our radial-profile analysis separates the 313 counts 1 within a source-centered circle of radius 1 arcsec into contributions of 90 per cent from unresolved emission and 10 per cent from the extended component. Spectral analysis supports the dominance of non-thermal emission in the unresolved component. The data give a good fit to a single-component absorbed power law, as shown

¹ Counts refer to 0.4–7 keV throughout §2.3.

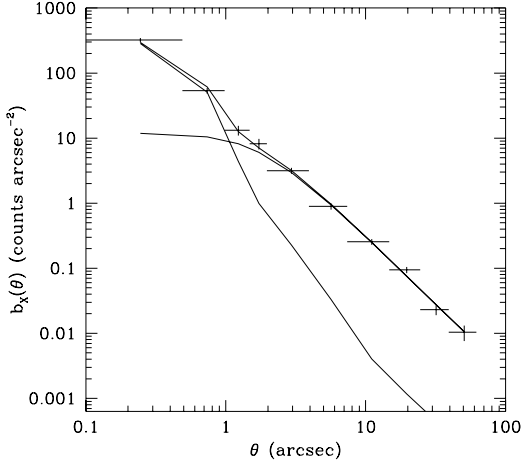


Figure 2. The data show the background-subtracted 0.4–7 keV radial profile, excluding a pie slice of position angle between 295° and 325° in order to avoid the resolved jet emission. The model is a composite of a β model and unresolved component: the individual components and the sum are shown as solid lines. The counts per unit area in a β model are proportional to $(1 + \theta^2/\theta_{\text{cx}}^2)^{0.5-3\beta}$, and the best fit values are $\beta = 0.515$, $\theta_{\text{cx}} = 1.55$ arcsec, $\chi_{\text{min}}^2 = 8.9$ for 6 degrees of freedom.

Table 1. Radial-profile analysis, 0.4–7 keV

Parameter	Value
point-source counts	380 ± 35
β	0.515 ± 0.03
Core radius, θ_{cx}	1.55 ± 0.7 arcsec
$\theta_{\text{FW10\%M}}$	9 ± 3 arcsec, 3.0 ± 1 kpc
β -model counts, $\theta < 10$ arcsec	409 ± 40
β -model counts, $\theta < 45$ arcsec	693 ± 44

Since parameters are correlated (β , θ_{cx}), (point-source counts, β -model counts), uncertainties are 1σ for two interesting parameters. $\theta_{\text{FW10\%M}}$ is the full width to 10 per cent of maximum of the β model. Counts have been multiplied by 360/330 to account for the excluded pie slice.

in Fig. 3. While the statistics are inadequate for fitting a two-component model, a single-component thermal model gives unrealistic results: a best-fitting temperature of 25 keV, an intrinsic absorption of $N_{\text{H}} = 4 \times 10^{21} \text{ cm}^{-2}$, and a 0.5–7 keV luminosity of $3 \times 10^{41} \text{ ergs s}^{-1}$ which is unreasonably high for the X-ray binary population within 335 pc of NGC 315’s centre.

To measure the spectrum of the extended emission we have fitted a Raymond-Smith thermal model to the 511 counts from a core-centred annulus of radii 2 arcsec and 45 arcsec, excluding a pie slice of position angle between 295° and 325° , to avoid the resolved jet emission and the majority of counts from the unresolved emission. The best fit gives $kT \approx 0.6$ keV and a small intrinsic absorption of $N_{\text{H}} = 5 \times 10^{20} \text{ cm}^{-2}$ (comparable to Galactic absorption), although the uncertainties are such that the additional absorption is consistent with being zero. There is marginal improvement in the fit (an F test giving a 7 per cent probability of the improvement in χ^2 being by chance) if a thermal bremsstrahlung component (best-fitting $kT = 4.2$ keV) is included in the model. In this case the minimum χ^2 is 20.8 for 17 degrees of freedom, and a 0.5–7 keV luminosity of $6 \times 10^{40} \text{ ergs s}^{-1}$ (about 20 per cent of the total luminosity from the region) is in the bremsstrahlung

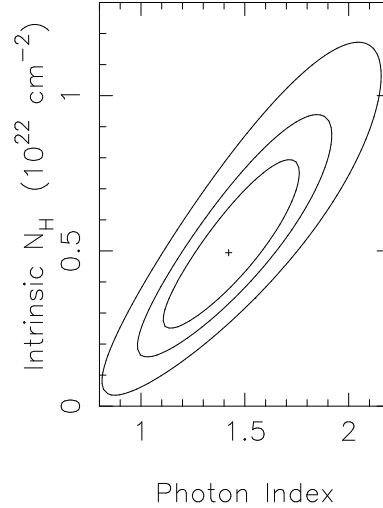


Figure 3. χ^2 contours (1σ , 90%, and 99%, for two interesting parameters) for a spectral fit to the nuclear X-ray emission extracted from a circle of radius 1 arcsec. The model is a single-component power law with intrinsic and (fixed) Galactic absorption. In the band 0.4–7 keV the spectrum contains 313 counts, and from the radial profile we expect roughly 10 per cent of these counts to be from the extended hot-gas component. $\chi_{\text{min}}^2 = 11.5$ for 13 degrees of freedom.

component. Although this is a factor of a few higher than expected for the composite emission from X-ray binaries in the NGC 315 galaxy, the uncertainties are large. The abundance of the thermal gas increases from about 0.2 solar to more reasonable values between about 0.5 and 1.0 solar when the bremsstrahlung component is included. A consistent temperature is found for the thermal gas, whether or not the bremsstrahlung component is included, and the statistical uncertainties dominate the errors. The best-fit value and 90 per cent confidence uncertainties (for one interesting parameter) are estimated to be $kT = 0.62 \pm 0.06$ keV.

Our spectral fitting to the total 920 counts in the central 2 arcsec radius core plus the region of the previous paragraph finds a two-component power-law plus thermal model to be acceptable. The statistical quality of the data is insufficient to require more complex spectral models, such as the addition of a bremsstrahlung component. The results are insensitive to the gas abundance (which we set to be 0.5 times solar) and intrinsic absorption in front of the thermal emission (which we set to be zero). The χ^2 contours of power-law slope versus gas temperature are shown in Fig. 4. For the best-fit parameters, the number of counts in the power-law component is 438 ± 38 (1σ statistical error only). This is in reasonable agreement with the results from the radial-profile analysis (Table 1). In the remainder of this paper the radial-profile analysis is used to separate the counts into unresolved emission, which we characterize by a power law of photon spectral index 1.4 ± 0.4 , from the resolved emission which we characterize by a thermal model with $kT = 0.6 \pm 0.1$ keV.

With so few counts, the spectrum of the resolved jet emission is poorly constrained. However, the distribution of counts suggests a spectrum which is steeper than that of the core. A formal fit (of the counts in four energy bins) with no intrinsic absorption gives a photon spectral index of 2.5 ± 0.7 (1σ uncertainty).

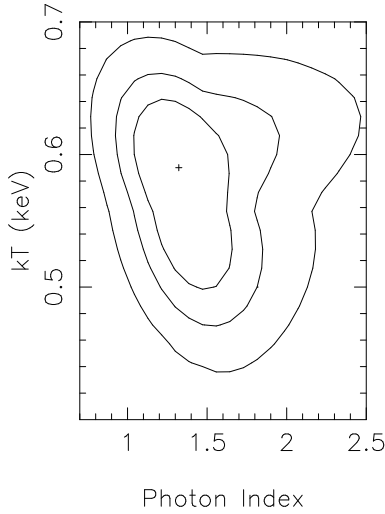


Figure 4. χ^2 contours (1σ , 90%, and 99%, for two interesting parameters) for a spectral fit to the X-ray emission from a circle of radius 45 arcsec, excluding a pie slice of position angle between 295° and 325° , to avoid the resolved jet emission. The model is the combination of a power law with intrinsic absorption and a thermal model, both with (fixed) Galactic absorption. $\chi^2_{\min} = 36.1$ for 33 degrees of freedom.

Table 2. X-ray components

Parameter	Value
Resolved Jet:	
L_x (0.4–5 keV)	3.5×10^{40} ergs s^{-1}
Core:	
L_x (0.4–5 keV)	5.3×10^{41} ergs s^{-1}
Gas:	
L_x (0.4–5 keV, $r \leq 15$ kpc)	3.6×10^{41} ergs s^{-1}
Density ($\theta = 0$)	$(3.4^{+1.5}_{-1.0}) 10^{-1}$ cm^{-3}
Density ($\theta = 10''$)	$(1.9 \pm 0.4) 10^{-2}$ cm^{-3}
Pressure ($\theta = 0$)	$(7^{+3}_{-2}) 10^{-11}$ Pa
Pressure ($\theta = 10''$)	$(4 \pm 1) 10^{-12}$ Pa
\dot{M} ($\theta \leq \theta_{cx}$)	$0.05 \pm 0.01 M_\odot$ yr^{-1}

Luminosities are before absorption. Multiply pressure values by 10 for units of dynes cm^{-2} , commonly quoted in X-ray astronomy papers. Uncertainties are 1σ for 1 interesting parameter. \dot{M} is the mass cooling rate of gas within the core radius. Uncertainties in the luminosities are dominated by the statistical uncertainties in the counts, given earlier in the paper.

2.4 Physical Parameters of the X-ray Components

In this short observation we have measured resolved jet emission between about 3 and 15 arcsec from the nucleus. The counts are converted into a 0.4–5 keV luminosity in Table 2 assuming a power law of photon spectral index 2.5. The 1 keV flux density is then 4.3 nJy. The 5 GHz radio flux from a matched region in the map of Fig. 1 is 68 mJy. The two-point rest-frame 5-GHz to 1-keV spectral index is therefore $\alpha_{rx} = 0.94 \pm 0.01$, where the error is dominated by the 16 per cent uncertainty in the X-ray counts (§2.1).

With regard to the core emission, the spectral index of the power-law component (Fig. 3) is highly correlated with the intrinsic absorption. Our results suggest a somewhat flatter spectral index and lower absorption than found by Matsumoto et al. (2001; spectral index of $2.02^{+0.37}_{-0.32}$, $N_H = 0.9^{+0.6}_{-0.5} \times 10^{22}$ cm^{-2}) in a two-component thermal and power-law fit to ASCA data, but the results are consistent with a similar correlation of spectral index and intrinsic absorption. Table 2 gives the best-fit 0.4–5 keV lumi-

osity of the power-law component. This is comparable with the luminosities of two other low-power radio galaxies from the B2 sample in which *Chandra* has found unresolved X-ray cores and resolved jets, B2 0206+35 at 2.9×10^{41} ergs s^{-1} and B2 0755+37 at 1.9×10^{42} ergs s^{-1} (Worrall et al. 2001). The 2–10 keV luminosity of NGC 315’s power-law component is 6.8×10^{41} ergs s^{-1} , larger than the ASCA value of 3.1×10^{41} ergs s^{-1} (Matsumoto et al. 2001) and possibly supporting variability similar to that reported between *ROSAT* PSPC and HRI observations by Worrall & Birkinshaw (2000). The interpolation to a 0.2–1.9 keV luminosity further supports variability of a factor of about 3 when compared with the *ROSAT* PSPC results (Worrall & Birkinshaw 2000), with *ROSAT* being higher, but this is highly dependent on the spectral index used for the interpolation, and a spectrum closer to the ASCA result removes the requirement for variability. The 2 keV core flux density from the *Chandra* observation is 40 nJy. Since this is the same value as adopted by Giovannini et al. (1994), their conclusions concerning relativistic beaming based on synchrotron self-Compton emission in the VLBI core would be unchanged.

Values for physical parameters of the X-ray-emitting gas are listed in Table 2. *Chandra*’s high spatial resolution finds a smaller core radius (Table 1) and a density gradient within 10 arcsec of the centre to which the *ROSAT* PSPC was insensitive, but the gas pressure at 10 arcsec is in remarkable agreement with the *ROSAT* results (compare Table 2 with figure 9 of Worrall & Birkinshaw 2000). When the best-fit *Chandra* results are extrapolated to estimate the gas luminosity for $\theta < 3$ arcmin and 0.2–2.5 keV, we find a value of 5.3×10^{41} ergs s^{-1} , which is in excellent agreement with the value of $(5.4 \pm 0.2) \times 10^{41}$ ergs s^{-1} from *ROSAT*, and the gas temperature (see Fig. 4) is also in good agreement with the value of $kT = 0.62^{+0.09}_{-0.1}$ keV from *ROSAT* (Worrall & Birkinshaw 2000). Our results for the temperature are lower than $kT = 0.8^{+0.04}_{-0.06}$ keV found from ASCA data by Matsumoto et al. (2001). While there is no obvious explanation for the difference, we note that while the ASCA data have more counts, the gas and AGN emission were both unresolved in the ASCA beam so that there was no ability to measure the spectrum of the gas uncontaminated by AGN emission, as is possible with *Chandra*. NGC 315’s 0.4–5 keV gas luminosity within a radius of 15 kpc is similar to the values of 2.6×10^{41} ergs s^{-1} and 4.2×10^{41} ergs s^{-1} found for B2 0206+35 and B2 0755+37, respectively (Worrall et al. 2001).

3 DISCUSSION

Chandra has

- (i) made the first detection of resolved X-ray jet emission in the nearby radio galaxy NGC 315,
- (ii) confirmed, with high spatial resolution, results from *ROSAT* and ASCA that the bulk of the X-ray emission is comprised of a combination of galaxy-scale emission, principally from a hot X-ray-emitting atmosphere, and unresolved emission which fits a power-law spectrum, and
- (iii) found evidence that the resolved X-ray jet is of steeper spectrum than the core, and that the jet emission is brightest close to the core, in particular at the base of the first bright radio knot.

The resolved jet emission has properties similar to those seen in deep observations of some other FRI sources. For example, the power-law energy spectral index of the X-ray emission, $\alpha_x = 1.5 \pm 0.7$, is consistent with the two-point radio to X-ray spectral index of 0.94, supporting a synchrotron origin with either a broken or

unbroken spectrum, depending on the radio spectrum in this region. Such a synchrotron spectrum would be consistent with Butcher et al. (1980)'s optical upper limit on jet emission of $1\mu\text{Jy}$ per kpc. The inverse Compton arguments applied to 3C 66B by Hardcastle et al. (2001) give similar results for NGC 315 in underpredicting the X-ray emission under reasonable assumptions for orientation, beaming, and available photon fields. The strong X-ray emission at the base of the first radio enhancement is a behaviour similar to that seen in 3C 66B (Hardcastle et al. 2001) and Cen A (Kraft et al. 2002).

When we compare the X-ray flux density of the unresolved emission with the total VLBI 5 GHz radio flux density of 477 ± 5 mJy from Venturi et al. (1993), we find a two-point rest-frame 5 GHz to 1 keV spectral index of $\alpha_{\text{rx}} \approx 0.86$. The uncertainties are dominated by possible variability, with the factor of three discussed in §2.4 leading to an uncertainty in α_{rx} of about ± 0.06 . The value of α_{rx} is within the range of 0.8 to 0.93 found for three other B2 bright-sample FRI radio galaxies observed with *Chandra* (Worrall et al. 2001). Similar values of α_{rx} for galaxies of different fluxes would support a relationship between the core radio and X-ray components, as argued statistically for the B2 bright sample based on *ROSAT* data by Canosa et al. (1999). The core two-point spectral index is somewhat flatter than that inferred for the resolved jet, possibly lending support to a different (inverse Compton) origin for the core emission (e.g., Giovannini et al. 1994, Hardcastle & Worrall 2000).

The nuclear X-ray emission of NGC 315 is seen through a moderate intrinsic column density (Fig. 3) of $N_{\text{H}} = (5_{-2.7}^{+3.2}) \times 10^{21} \text{ cm}^{-2}$ (90 per cent confidence uncertainty for 1 interesting parameter). *Chandra* typically finds intrinsic column densities below 10^{22} cm^{-2} in FRI radio-galaxy nuclei (e.g., Worrall et al. 2001; Hardcastle et al. 2001, 2002; Wilson & Yang 2002). Nuclear optical emission, now commonly detected with HST, has been shown by Chiaberge, Capetti & Celotti (1999) to correlate with the VLA-scale core radio emission. This optical emission is generally associated with extinction at a level compatible with the X-ray absorption (e.g., Ferrarese & Ford 1999), suggesting that both the X-ray and optical emission are associated with the sub-kpc-scale radio jets (Hardcastle & Worrall 2000).

It is unclear whether FRI radio galaxies contain a dense torus of gas and dust of the type required by models which unify powerful radio sources (Barthel 1989). Cen A and NGC 4261 are the clearest cases where column densities of order 10^{23} cm^{-2} are required by the X-ray data (Kraft et al. 2003, in preparation; Zezas et al. 2003). Both objects are closer than NGC 315, with the advantage that the nuclear emission is better separated from kpc-scale, radio-related, X-rays. However, M 87 is also nearby and does not require a heavily-absorbed component (Wilson & Yang 2002). Even if central tori exist in FRI radio galaxies, most of the X-ray emission may be associated with structures on larger scales, since there is at least one good case where the nucleus is known to be radiatively inefficient (Di Matteo et al. 2003). Little or no excess nuclear absorbing column would then be seen, except in cases (such as NGC 4261) where the jets lie almost in the plane of the sky. If this is the case, the low X-ray column density of NGC 315, whose jets may lie $\sim 35^\circ$ from the line of sight (see §1), says little about the presence or absence of a nuclear torus, although a second, heavily-absorbed, component might appear in a deeper X-ray observations.

We have compared the pressure in the radio jet with that in the external X-ray emitting gas, assuming an equipartition magnetic field. At 10 arcsec from the core the FWHM of the radio jet is roughly 1.3 arcsec. Using the radio flux density in a cylin-

der of length 1 arcsec, modelling the electron spectrum above $\gamma_{\text{min}} = 10$ with a synchrotron spectrum consistent with the distribution of radio, X-ray, and optical (upper limit) flux densities over the surrounding 12-arcsec length of jet, assuming no relativistic protons, a filling factor of unity, no relativistic bulk motions, and a jet on the plane of the sky, we find a pressure of about $6 \times 10^{-12} \text{ Pa}$, which is a reasonable match to the external pressure of $(4 \pm 1) \times 10^{-12} \text{ Pa}$ (Table 2) given the measurement and model uncertainties. Such a model would be appropriate if the radio source is intrinsically one-sided. If at 10 arcsec from the core the jet is inclined at $\theta = 35$ degrees to the line of sight, and has a bulk velocity of $0.7c$ (see §1), then the bulk relativistic beaming factor, $\delta = 1/\gamma(1 - \beta \cos \theta) = 1.67$. The minimum pressure in the jet will now be reduced, by a factor of roughly $\delta^{-10/7}(\sin \theta)^{4/7}$ (Bicknell 1994), i.e., to $2 \times 10^{-12} \text{ Pa}$. Projection effects mean that the jet is longer. The pressure in a β -model external atmosphere scales as $(\cos \theta)^{3\beta}$ at large distances from the core radius, i.e., to give $\approx 2.9 \times 10^{-12} \text{ Pa}$, such that a match between minimum jet pressure and external pressure can still be claimed given the uncertainties. Pressure balance between the external medium and the minimum pressure in the jet at about 100 arcsec from the core (on the reasonable assumption that the jet is now sufficiently slow that beaming can be ignored) has previously been reported based on *ROSAT* PSPC data by Worrall & Birkinshaw (2000), who point out that NGC 315 appears to be rather different from other B2 bright sample radio galaxies in remaining in pressure balance (at minimum pressure) over a large length of radio jet, without requiring an additional component of internal pressure.

REFERENCES

- Barthel, P.D., 1989, *ApJ*, 336, 606
 Bicknell, G.V., 1986, *ApJ*, 305, 109.
 Bicknell, G.V., 1994, *ApJ*, 422, 542.
 Birkinshaw, M., 1994, in Crabtree, D.R., Hanisch, R.J., Barnes, J., eds., ASP Conference Series, Vol. 61, p. 249
 Bridle, A.H., Davis, M.M., Fomalont, E.B., Willis, A.G., Strom, R.G., 1979, *ApJ*, 228, L9.
 Butcher, H.R., van Breugel, W., Miley, G.K., 1980, *ApJ*, 235, 749
 Canosa, C.M., Worrall, D.M., Hardcastle, M.J., Birkinshaw, M., 1999, *MNRAS*, 310, 30
 Chiaberge, M., Capetti, A., Celotti, A., 1999, *A&A*, 349, 77
 Colla, G., Fanti, C., Fanti, R., Gioia, I., Lari, C., Lequeux, J., Lucas, R., Ulrich, M.-H., 1975, *A&A*, 38, 209
 Cotton, W.D., Feretti, L., Giovannini, G., Lara, L., Venturi, T., 1999, *ApJ*, 519, 108
 de Ruiter, H.R., Parma, P., Capetti, A., Fanti, R., Morganti, R., 2002, *A&A*, 396, 857
 Dickey, J.M., Lockman, F.J., 1990, *ARA&A*, 28, 215
 Di Matteo, T., Allen, S.W., Fabian, A.C., Wilson, A.S., Young, A.J., 2003, *ApJ*, 582, 133
 Fanaroff, B.L., Riley, J.M., 1974, *MNRAS*, 167, 31p
 Ferrarese, L., Ford, H.C., 1999, *ApJ*, 515, 583
 Giovannini, G., Feretti, L., Venturi, T., Lara, L., Marcaide, J., Rioja, M., Spangler, S.R., Wehrle, A.E., 1994, *ApJ*, 435, 116
 Giovannini, G., Cotton, W.D., Feretti, L., Lara, L., Venturi, T., 2001, *ApJ*, 552, 508
 Hardcastle, M.J., Worrall, D.M., 2000, *MNRAS*, 314, 359
 Hardcastle, M.J., Birkinshaw, M., Worrall, D.M., 2001, *MNRAS*, 326, 1499
 Hardcastle, M.J., Worrall, D.M., Birkinshaw, M., Laing, R.A., Bridle, A.H., 2002, *MNRAS*, 334, 182
 Kraft, R.P., Forman, W.R., Jones, C., Murray, S.S., Hardcastle, M.J., Worrall, D.M., 2002, *ApJ*, 569, 54.

- Matsumoto, Y., Fukazawa, Y., Nakazawa, K., Iyomoto, N., Makishima, K., 2001, PASJ, 53, 475
- Schreier, E.J., Feigelson, E., Delvaille, J., Giacconi, R., Grindlay, J., Schwartz, D.A., Fabian, A.C., 1979, ApJ, 234, L39
- Schreier, E.J., Gorenstein, P., Feigelson, E.D., 1982, ApJ, 261, 42
- Ulrich, M.-H., 1989, in Maraschi, L., Maccacaro, T., Ulrich, M.-H., eds, BL Lac Objects, Springer-Verlag, Berlin, p. 45.
- Venturi, T., Giovannini, G., Feretti, L., Comoretto, G., Wehrle, A.E., 1993, ApJ, 408, 81
- Verdoes Kleijn, G.A., Baum, S.A., de Zeeuw, P.T., O'Dea, C.P., 1999, AJ, 118, 2592
- Wilson, A.S., Yang, Y., 2002, ApJ, 568, 133
- Worrall, D.M., Birkinshaw, M., 1994, ApJ, 427, 134
- Worrall, D.M., Birkinshaw, M., 2000, ApJ, 530, 719
- Worrall, D.M., Birkinshaw, M., Hardcastle, M.J., 2001, MNRAS, 326, L7
- Xu, C., Baum, S.A., O'Dea, C.P., Wrobel, J.M., Condon, J.J., 2000, AJ, 120, 2950
- Zezas, A., Birkinshaw, M., Worrall, D.M., Peters, A., Fabbiano, G., 2003, ApJ, submitted